IEEE Photonics Journal
An IEEE Photonics Society Publication

Open Access

A Highly Sensitive SPR Sensors Based on Two Parallel PCFs for Low Refractive Index Detection

Volume 10, Number 4, August 2018

Famei Wang
Chao Liu
Zhijie Sun
Tao Sun
Banghua Liu
Paul K. Chu

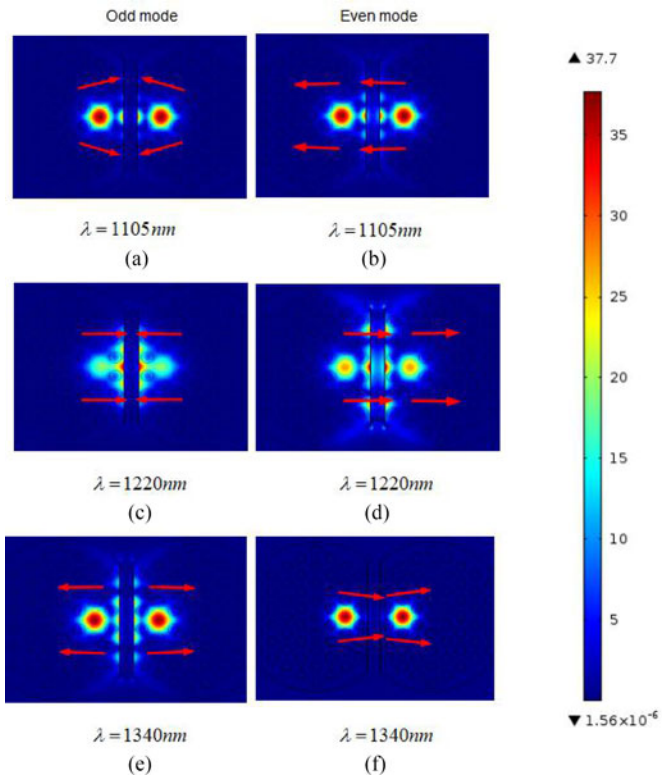

DOI: 10.1109/JPHOT.2018.2856273
1943-0655 © 2018 IEEE

IEEE photonics SOCIETY

IEEE

A Highly Sensitive SPR Sensors Based on Two Parallel PCFs for Low Refractive Index Detection

Famei Wang,[1] Chao Liu,[2] Zhijie Sun,[1] Tao Sun,[3] Banghua Liu,[4] and Paul K. Chu[5]

[1]Institute of Materials Processing and Intelligent Manufacturing, Center for Biomedical Materials and Engineering, Harbin Engineering University, Harbin 150001, China
[2]School of Electronics Science, Northeast Petroleum University, Daqing 163318, China
[3]Institute of Microelectronics, Agency of Science, Technology and Research (A*STAR), Singapore 117685
[4]Institute of Planning and Design, Natural Gas Company, Daqing Oil Field Limited Company, Daqing 163000, China
[5]Department of Physics and Materials Science, City University of Hong Kong, Hong Kong

DOI:10.1109/JPHOT.2018.2856273

Manuscript received June 13, 2018; revised July 8, 2018; accepted July 11, 2018. Date of publication July 16, 2018; date of current version July 23, 2018. This work was supported by the National Natural Science Foundation of China under Grant 51474069, in part by the China Postdoctoral Science Foundation funded project under Grant 2016M591510, in part by the Natural Science Foundation of Heilongjiang Province under Grant E2016007, and in part by the City University of Hong Kong Applied Research Grant under Grant 9667122. Corresponding author: Chao Liu (e-mail: msm-liu@126.com).

Abstract: Based on two parallel photonic crystal fibers (PCFs) with D-shape structure, a novel surface plasmon resonance (SPR) sensor with low refractive index (RI) detection at near-infrared wavelengths is described. According to the coupled-mode theory, directional power transfer between the two fiber cores is enhanced by resonant coupling between the surface plasmon modes and fiber core-guided modes. In comparison with corresponding single D-shape PCF, a maximum spectral sensitivity up to 13 500 nm/RIU and resolution of 7.41×10^{-6} RIU for RI detection range between 1.27 and 1.32 are achieved. The proposed two parallel D-shape PCFs-SPR sensor with lower RI detection range offer large potential in the fields of pharmaceutical inspection and pharmaceutical leakage monitoring.

Index Terms: PCF-SPR, parallel fiber, near-infrared, lower RI detection.

1. Introduction

Surface plasmon resonance is an effective sensing technology and has been widely applied in biotechnology, medical diagnostics, and environmental monitoring own to its extreme sensitivity to refractive index variations [1]–[3]. Based on optical fiber SPR sensors, the D-shape [4], cladding-off [5], single mode fiber (SMF) [6], Bragg grating fiber [7], and photonic crystal fiber (PCF) [8]–[10] have been demonstrated theoretically and experimentally. Among them, PCF based-SPR (PCF-SPR) sensors have a great deal of advantages over conventional optical fiber SPR sensors including small size, flexible structural design, high sensitivity, and phase-matching condition. To implement PCF-SPR sensors, the metal layers and the analyte usually must be filled inside the fiber but the analyte in the PCF holes is difficult to change. In order to enhance the penetration of metal coating and sensing media inside the fiber, the sensing method of an external coating PCF has been

put forward. Metal layers/sensing media have been placed outside the fiber, which simplifies the fabrication process and sensing mechanism [11].

Spurred by advances in micro-fabrication technology, the D-shape PCFs are experimentally available. The D-shape PCF-SPR have attracted much interest for their unique performances [12], [13]. N. Luan *et al.* [14] proposed the D-shaped hollow core PCF-SPR sensor and investigated the effect of air holes on the SPR sensing performance. The wavelength sensitivity of 2900 nm/RIU was achieved for RI (1.33,1.34) detection. J.N. Dash and R. Jha described a D-shape PCF-SPR sensor in which a silver-graphene layer as the sensitive materials was coated outside the fiber structure [15]. The amplitude sensitivity was 216 RIU^{-1} with the spectral sensitivity of 3700 nm/RIU for RI detection range in 1.33-1.37. G. An *et al.* [16] developed a D-shape PCF-SPR sensor with a rectangular lattice, and the plane of the polished fiber coated the nanoscale gold film. The maximum spectral sensitivity of the sensor in the RI range between 1.33 and 1.35 is about 2000 nm/RIU. One of the advantages of the D-shaped PCF-SPR sensors is that the sensitive metal layer can be coated adjacent to the core, which promotes strong interaction with the analyte, and results in enhanced sensing performance. The interaction between the plasmonic mode and fundamental mode depends on the structural parameters of the sensors. The coupling enhancement effect is not effective for some single D-shape PCF-SPR sensors due to the complicated structure [17]. However, it is an effective approach to enhance the coupling effects between the plasmonic mode and fundamental core guided mode by using two parallel D-shape PCFs. Most of the mode operations for reported D-shaped PCF-SPR sensors have been carried out in the visible wavelength range and RI range larger than 1.33, but relatively little efforts have been devoted to use two parallel fibers for lower RI detection (1.27–1.33). For many halogenated ethers and pharmaceuticals, their refractive indexes are located in the lower RI range [18], [19]. Therefore, the sensors with lower RI detection range offer great potential in the fields of pharmaceutical inspection and pharmaceutical leakage monitoring [20].

In this work, a novel SPR sensor based on parallel double D-shaped PCFs with a high sensitivity at near-infrared wavelengths is proposed and numerically analyzed. By using finite-element method (FEM), the characteristics of the sensor are numerically studied. The performance of a conventional D-shape PCF-SPR sensor is compared to that of the D-shape PCFs-SPR parallel-detection sensor. The results show that the maximum spectral sensitivity of 13500 nm/RIU is attained for the RI range from 1.27 to 1.32 and the resolution is 7.41×10^{-6} RIU.

2. Materials and Methods

The original structure of the sensor is shown in Fig. 1(a). The sensor is composed of four layers of air holes arranged in a hexagonal lattice and the gold layer is coated on the surface of the PCF plane. Gold and silver are extensively used as plasmonic materials. Although silver possesses a sharper resonance peak than gold, it is unstable and easily oxidized. Therefore, gold is chosen as the surface plasmon layer due to its chemical stability in this work. Compared to the micro-structured PCF coated with metal inside of the air holes, this sensor avoids the inhomogeneity of the gold layer. This D-shape PCF-SPR sensor contacts the analyte via the gold layer rather than requiring the analyte to fill the small air holes. The thickness of the gold layer is $t_{Au} = 50$ nm and the length of the gold layer is 6.5 μm. The dielectric constant of gold is expressed as [21]:

$$\varepsilon_{Ag}(\omega) = \varepsilon_{\infty} - \frac{\omega_p^2}{\omega(\omega + i\omega_\tau)}, \tag{1}$$

where $\varepsilon_{\infty} = 9.75$, $\omega_p = 1.36 \times 10^{16}$, $\omega_c = 1.45 \times 10^{14}$ is the dielectric constant, the plasma frequency, and the scattering frequency of gold, respectively.

It is well-known that the structure parameters have great influences on the performances of the sensors. Based on numerous simulations, the dimension parameters of the proposed two D-shaped PCFs-SPR sensor are determined as follows. The diameter of each D-shaped PCF is 9 μm, and the diameter of the perfectly matched layer (PML) is 11 μm. The pitch size of the cladding air hole is $\Lambda = 1$ μm, the diameters of the air hole is $d_a/\Lambda = 0.6$, and the distance between the two D-shape

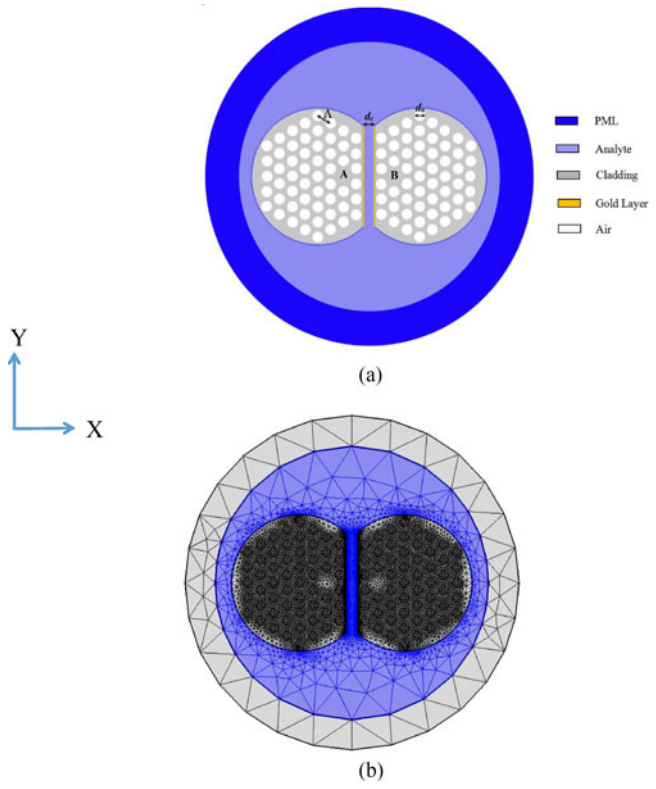

Fig. 1. (a) Original cross-sectional structure and (b) FEM mesh of the proposed sensor.

fibers is $d_c/\Lambda = 0.8$. RI of the analyte (n_c) is 1.27–1.32 and $n_a = 1.0$ is air RI. In the theoretical analysis, the D-shape fibers are considered to be made of silica glass and the RI of silica glass is calculated by the Sellmeier equation [22]:

$$n^2 - 1 = \frac{0.6961663\lambda^2}{\lambda^2 - (0.0684043)^2} + \frac{0.4079426\lambda^2}{\lambda^2 - (0.1162414)^2} + \frac{0.897479\lambda^2}{\lambda^2 - (9.896161)^2}, \tag{2}$$

With regards to fabrication, the required D-shaped PCFs have been achieved by widely known etching or side polishing technique and have been reported in many literatures such as Ref. [13], thus the fabrication technology for D-shaped PCFs is available. Then the high pressure chemical vapor deposition (CVD) technique could be used to deposit metal layers on the plane of the D-shaped PCFs and offers good control of the outer metal layer thicknesses, allowing for uniformity along the whole fiber length [23]. It can be accomplished by accurately adjusting the distance between the two D-shaped PCFs with microscopy and fixed with the precision instruments. Although it is slightly difficult to manipulate the two D-shaped PCFs adjacent each other at nanoscale, yet it is reasonable to believe that this difficulty can be overcome under the assistance of modern nano-manufacturing technology.

For the D-shape fiber based on SPR sensing, the propagation loss α_{loss} is defined as [24]:

$$\alpha_{loss} = \frac{40\pi}{\lambda \ln 10} \mathrm{Im}\left(n_{eff}\right) \times 10^6 \left(dB/m\right) \approx 8.686 \mathrm{Im}\left(n_{eff}\right) 2\pi/\lambda, \tag{3}$$

The propagation loss of the sensor are numerically investigated by the FEM [24]. Fig. 1(b) shows the cross-sectional FEM mesh of the sensor. The calculating area is made of 14516 meshes, and a perfectly matched layer (PML) has 7293 elements. The vertex number is 466 and the minimum unit is $5.351e^{-6}$ in the structure.

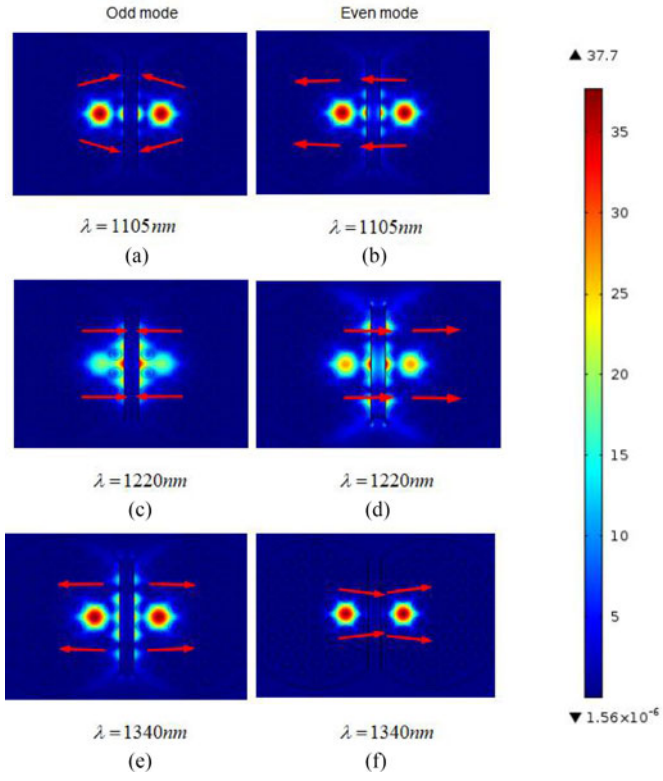

Fig. 2. Electric field distributions of the core-guided mode for the odd mode at (a) 1105 nm, (c) 1220 nm, and (e) 1340 nm and electric field distributions of the core-guided mode for the even mode at (b) 1105 nm, (d) 1220 nm, and (f) 1340 nm.

3. Results

Fig. 2(a)–(f) display the electric field distributions of the core-guided mode for the even mode and odd mode at specific wavelengths. The scale bar in this figure represents the magnitude of the electric field. The red area is the largest distribution of light energy and the blue is the smallest distribution of light energy. Fig. 2(a)–(e) show most of the light energy distributes in the two cores and the metal surface. The light energy distributions of the core-guided mode are limited to the fiber core as shown in Fig. 2(f). The arrows represent the direction of the electric field. It can be obviously observed from Fig. 2 that light energy is transferred between the two cores, leading to improved strong-interaction coupling at the metal surface. There are no y-polarized modes as the geometrical fibre structure is not symmetrical in the x and y dimensions and the light energies between two fibers periodically change only in the direction of the x polarization. For the uncoated gold layer parallel D-shape PCFs, the total interference transverse electric field $\vec{E}(x, y, z)e^{-jwt}$ can be given as [25]:

$$\vec{E}\,(x, y, z)\, e^{-jwt} = \left[M\,(x, y, z)\, e^{j\phi(x,y,z)}\right] e^{j[(\beta_e+\beta_o)/2z-wt]}, \tag{4}$$

where $M = \sqrt{c_e^2E_e^2 + c_o^2E_o^2 + 2c_ec_oE_eE_o\cos[(\beta_e - \beta_o)z]}$ is the amplitude, $\varphi = \tan^{-1}[\frac{c_eE_e - c_oE_o}{c_eE_e + c_oE_o} \times \tan(\frac{\beta_e-\beta_o}{2}z)]$ is the phase shift, βe and βo are the propagating constants of the fiber core-guided even and odd modes, respectively, and $c_e^2 + c_o^2 = 1$.

The power of the two cores P_A and P_B is given by:

$$\begin{cases} P_A\,(z) = M^2\,(-x, y, z)\, c_e^2E_e^2\,(-x, y) + c_o^2E_o^2\,(-x, y) + 2c_ec_oE_e\,(-x, y)\,E_o\,(-x, y)\cos\,[(\beta_e - \beta_o)\,z] \\ P_B\,(z) = M^2\,(x, y, z)\, c_e^2E_e^2\,(x, y) + c_o^2E_o^2\,(x, y) - 2c_ec_oE_e\,(x, y)\,E_o\,(x, y)\cos\,[(\beta_e - \beta_o)\,z] \end{cases} \tag{5}$$

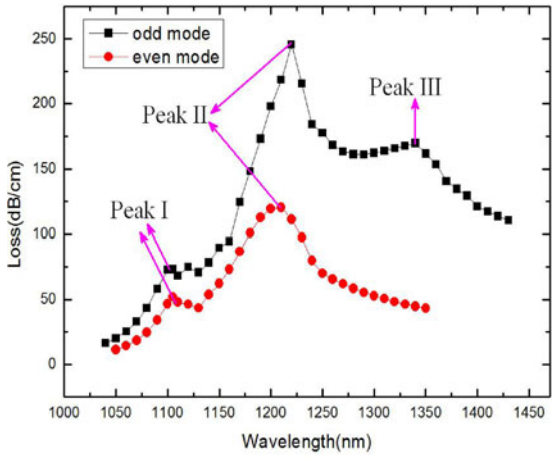

Fig. 3. Variation of the propagation loss depending on in the even and odd modes.

Given that $E_e(-x, y) = E_e(x, y)$ and $E_o(-x, y) = -E_o(x, y)$, the transmission characteristics of the parallel D-shape PCF-SPR sensor can be derived for the parallel D-shape PCF coated with a gold layer.

The transmittance function T'(z) is expressed as the ratio of the power transmitted from one core to another core and written as:

$$\begin{cases} T'(z) = \frac{P'_A(z)}{P'_B(0)} = \left[\frac{\psi(z)}{2}\right]^2 + \varphi(z) \times \sin^2\left(\frac{\beta_e - \beta_o}{2} z\right) \\ \psi(z) = 10^{-(\alpha_e z/20)} - 10^{-(\alpha_e z/20)}, \varphi(z) = 10^{-[(\alpha_e + \alpha_o) z/20]} \end{cases}, \tag{6}$$

For clarity and simplicity, we assume $c_e = c_o$ and $E_e = E_o$. z is the propagation length of the optical fiber. When z equals to zero, the optical power is mainly concentrated in the core B. Therefore, we can indicate that the incident energy is emitted in the core B and then transferred to the core A. The light energy is exchanged periodically between the two modes and so the amplitude of the two modes also changes periodically. During the periodic exchange of light energy between two fibers, more light energy coupled to the metal surface results in higher sensing sensitivity [25], [26].

Fig. 3 shows that the core-guided mode loss spectra for the odd mode and even mode of x-polarization. The black line and red line represent the loss spectra of the core-guided odd mode and even mode, respectively. There are three peaks in the spectra. The corresponding electric field distributions of the three resonant peaks as shown in Fig. 2(a)–(e). The peak with the largest propagation loss is denoted as the main peak and the others are designated as the secondary peaks. The peak in the loss spectrum of the core-guided mode indicates the resonant wavelength because the maximum energy is shifted from the core-guided mode to plasmonic mode at this wavelength. Several resonance peaks emerge due to coupling of the core-guided mode with higher order plasmonic modes [27]. In this study, the main peak is studied and more suitable for sensing detection because its resonant peak is the strongest. Fig. 2(c) and (d) show that the transferred energy of the odd mode at 1220 nm is more than that of the even mode. Fig. 3 further reveals a sharp loss peak at 1220 nm for the dispersion relations of the odd mode. The resonance intensity and depth of the odd mode are larger than those of the even mode. The resonance coupling of the odd mode at 1220 nm is stronger than that of the even mode. Therefore, the odd mode for x-polarization is selected to evaluate the performance of the proposed sensor in the subsequent analysis. Moreover, the resonance peak around 1220 nm is chosen for discussion because of its narrower bandwidth and higher resolution.

Fig. 4 displays the propagation loss spectra of the core-guided odd mode with the analyte RI range between 1.27 and 1.32. This refractive index range is located in the range of $1.27 < n < 1.35$ for biosensing detection [28]. The resonance wavelength shows the right move and the resonance

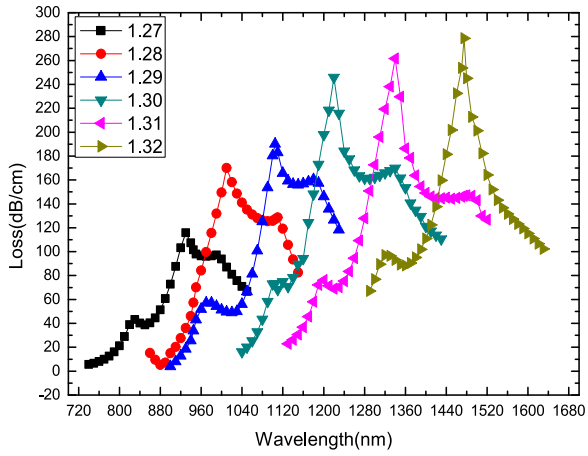

Fig. 4. Loss spectra of the core-guided odd mode of the sensor for analyte RI between 1.27 and 1.32.

depth increases with increasing analyte RI. It can be explanation that the absorption of gold layer relies on the environmental medium RI, the variation in absorption wavelength can be measured even if the change of sample RI is slight. Sensitivity is one of the important performance indicators of the sensor and needs to be evaluated in the analyte RI range. The spectral sensitivity S is shown as [29]:

$$S(\lambda) = \frac{\Delta\lambda_{peak}}{\Delta n_a}(\mathrm{nm}/RIU), \tag{7}$$

The maximum variation in resonance wavelength is $\Delta\lambda_{peak} = 135$ nm and the maximum spectral sensitivity of 13500 nm/RIU is obtained when the change of the analyte RI is $\Delta n_a = 0.01$. The wavelength resolution of the detector is assumed to be $\Delta\lambda_{\min} = 0.1$ nm and the RI resolution is represented as [30]:

$$R = \Delta n_a \Delta\lambda_{\min}/\Delta\lambda_{peak}. \tag{8}$$

Hence, assuming that the wavelength resolution of the detector for$\Delta\lambda_{\min} = 0.1$ nm, the RI resolution of the sensor is estimated to be about 7.41×10^{-6}RIU.

Consider a signal to noise ratio (SNR) of 60 dB, the minimum full-width-at-half-maxima(FWHM) is 72.5 nm for $n_a = 1.32$, a sensitivity of 13500 nm/RIU in 1.27–1.32 is obtained using a rigorous definition for the detection limit of the SPR sensor proposed in Ref. [8] (($\sigma n = FWHM/(4.5 \times S \times SNR^{0.25})$)), a high sensing resolution of 4.29×10^{-4} RIU is achievable.

For comparison, the cross-section and FEM mesh of the single D-shape PCF-SPR sensor are shown in Fig. 5. The structure of the single D-shape PCF-SPR sensor is the same as that of the parallel two D-shape PCFs. Figure 6 presents influence of the propagation loss with analyte RI between 1.29 and 1.32 for the single D-shape PCF-SPR sensor polarized along the x-axis. The resonance wavelength shows red shift and the resonance intensity increases when analyte RI from 1.29 to 1.32. Most of the energy is shifted from the fiber core to metal surface as shown in Fig. 6 [inset(b)]. In Fig. 6 [inset(a)] shows that the electric field distributions of the core-guided mode for the analyte RI $n_a = 1.30$, and almost all of the energy is concentrated in the fiber core outside the resonant wavelength. The maximum variation in resonance wavelength is $\Delta\lambda_{\mathrm{peak}} = 30$ nm and the maximum spectral sensitivity of 3000 nm/RIU is achieved. For the single D-shape sensor, the light energy is only in the single x-direction shifted from the core-guided mode to plasmonic mode. In comparison, for the parallel two D-shape sensor, the light energy is transferred from core A to core B and the amplitude of the two modes changes periodically. Therefore, more power is transferred to the plasmonic mode resulting in greater efficiency and intensity of resonance coupling. It can be seen that the sensing property of the parallel two D-shape PCFs is superior to that of the single

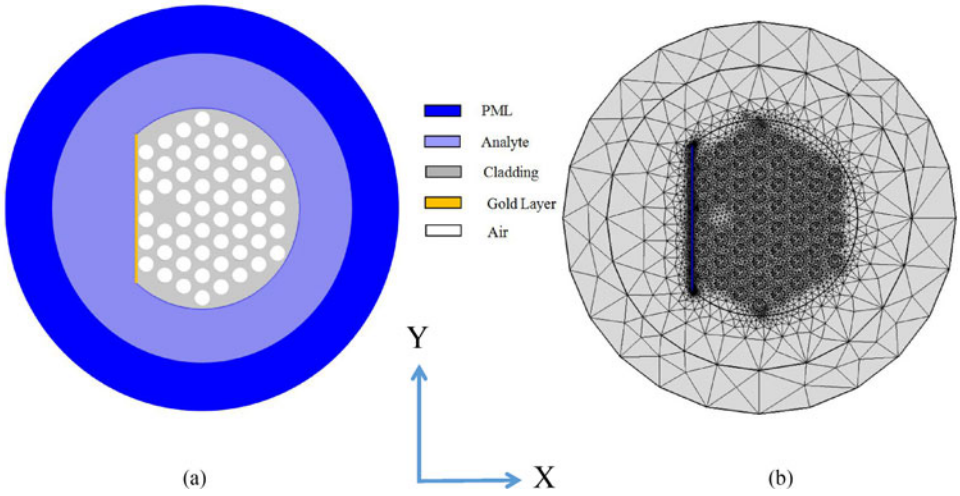

Fig. 5. (a) Cross-section structure and (b) FEM mesh of the single D-shape PCF-SPR sensor.

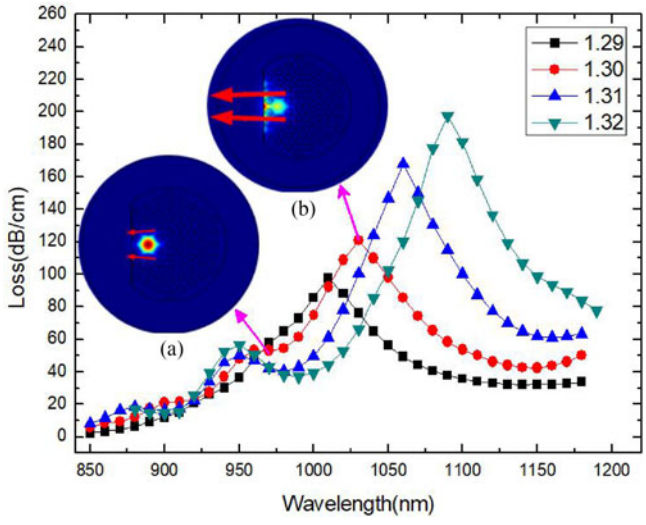

Fig. 6. Propagation loss curves of x-polarization mode for analyte RI between 1.29 and 1.32 of the single PCF with insets (a) and (b) showing the field distributions at different wavelengths.

D-shape PCF. Table 1 lists the key parameters for the sensing performance of PCF-SPR sensors with different structures. It is seen from Table 1 that the performance of the proposed parallel two PCFs-SPR sensor is not only better than that of the single D-shape PCF-SPR sensor, but also higher than that of other sensors.

The effects of geometrical parameters on the parallel two PCFs-SPR sensor are investigated while the other parameters are kept the same. Fig. 7 describes the propagation loss of the odd mode for different thicknesses of the gold layer (tAu) between 30 nm and 60 nm. A slight blue-shift occurs and the resonance peaks reduces gradually when the thickness of the gold layer is increased. Consequently, it is possible to tune and optimize the sensor performance such as the operation range and amount of loss precisely by adjusting the thickness of the gold layer [31]. It is seen from Fig. 7 that the propagation loss decreases with increasing the thickness of gold layer. The resonance peak of the 50 nm layer is sharper than that of the 30 nm layer, indicating the sensor possesses a higher sensitivity for the 50 nm gold layer. Therefore, the thickness of gold layer is determined to be 50 nm in the following discussion.

Table 1
Key Parameters Associated With the Sensing Performance of Various PCF-SPR Sensors

Fiber structure	Detection RI range (RIU)	Operation Wavelength range(nm)	Average Sensitivity (nm/RIU)	Ref.
Multi-core flat, PCF-SPR	1.46-1.485	1240-1420	9600	[3]
Simple D-shape, PCF-SPR	1.33-1.43	550-1770	9800	[12]
MOF, PCF-SPR	1.33-1.34	550-750	2900	[14]
Silver-Graphene D-shape, PCF-SPR	1.33-1.37	480-660	3700	[15]
Parallel two D-shape , PCF-SPR	1.27-1.32	720-1680	13500	This work

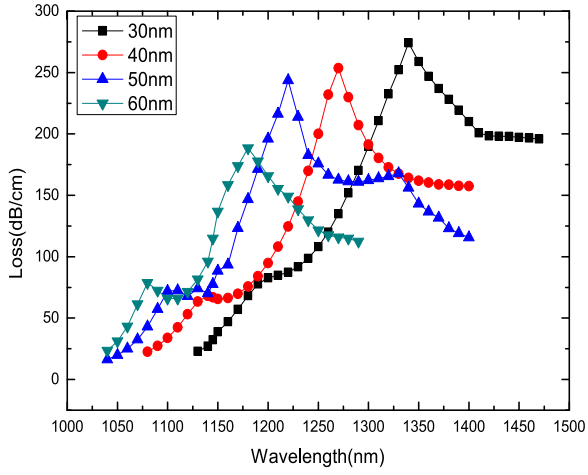

Fig. 7. Influence of the propagation loss with thicknesses of gold layers between 30 nm and 60 nm ($d_a/\Lambda = 0.6$, $d_c/\Lambda = 0.8$, and $n_a = 1.30$).

The distance between the parallel two fibers is one of important factors determining the sensitivity and resolution. Fig. 8 shows the propagation loss curves of different distances between two D-shape fibers. A slight red-shift occurs when d_c/Λ ranges from 0.4 to 1.2. The resonance intensity increases when d_c/Λ changes from 0.4 nm to 0.8 nm, while the resonance intensity decreases with d_c/Λ increasing from 0.8 to 1.2. This can be explained by the following reasons. Firstly, when the distance is smaller, the parallel two D-shape fibers are similar to a single dual-core fiber and the

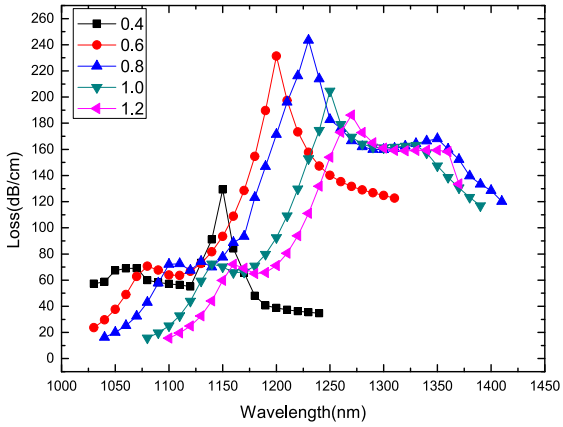

Fig. 8. Propagation loss curves of the core-guided mode depend on different distances for the parallel D-shape sensors ($d_a/\Lambda = 0.6$, $t_{Au} = 50$ nm, and $n_a = 1.30$).

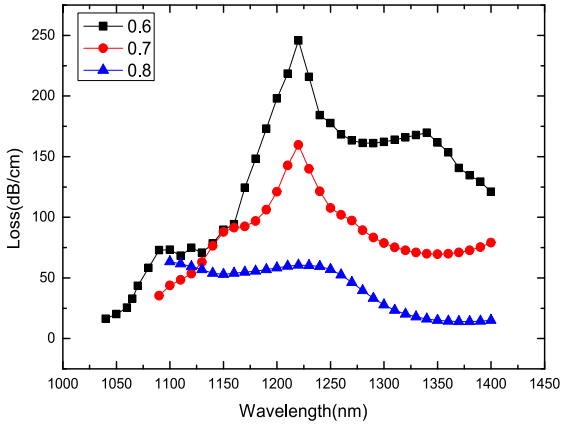

Fig. 9. Propagation loss curves of different air hole diameters ($d_c/\Lambda = 0.8$, $t_{Au} = 50$ nm, and $n_a = 1.30$).

resonance intensity is weaker because the coupling interaction is dominated by the coupling of the core-guided mode and plasmonic mode in single dual-core structure. Secondly, when the distance increases, the periodic couplings between two fibers increase gradually besides the coupling effect of the core-guided mode and plasmonic mode, leading to the intensity increasing of total couplings. Lastly, the interaction effects of the periodic couplings between two fibers decrease with the further increasing of the distance, which is similar to the case of two independent single fibers. Hence, 0.8 is chosen as the distance in our analysis.

Fig. 9 shows the propagation loss curves of the odd mode for the parallel D-shape sensors when d_a/Λ between 0.6 and 0.8. The resonance wavelength hardly moves and the resonance depth decreases with increasing d_a/Λ. This means that for a smaller air hole, more energy is accumulated in the fiber core. Therefore, the coupling effect of the core-guided mode and plasmonic mode decrease gradually with increasing d_a/Λ resulting in less propagation loss.

4. Conclusion

A parallel dual D-shape PCF-SPR sensor for near-infrared wavelengths is described and resonance coupling is studied systematically. Light energy is shifted from core A to core B and exchanged periodically between the two modes. The sensing performance of the proposed sensor is improved because the amplitude of the two modes changes periodically and more core energy is transferred to the surface plasmonic energy. For the RI range from 1.27 to 1.32, the maximum spectral sensitivity

of 13500 nm/RIU and the resolution of 7.41 $\times$ 10^{-6} RIU are achieved. The proposed PCFs-SPR sensor has promising applications in drug inspection and monitoring.

References

[1] R. C. Jorgenson and S. S. Yee, "A fiber-optic chemical sensor based on surface plasmon resonance," *Sens. Actuators B*, vol. 12, pp. 213–220, 1993.
[2] L. W. Chi and M. Olivo, "Surface plasmon resonance imaging sensors: a review," *Plasmonics*, vol. 9, pp. 809–824, 2014.
[3] A. A Rifat, G. A. Mahdiraji, Y. M. Sua, R. Ahmed, Y. G. Shee, and F. R. M. Adikan, "Highly sensitive multi-core flat fiber surface plasmon resonance refractive index sensor," *Opt. Express*, vol. 24, pp. 2485–2495, 2016.
[4] H. H. Qazi, A. B. Mohammad, H. Ahmad, and M. Z. Zulkifli, "D-Shaped polarization maintaining fiber sensor for strain and temperature monitoring," *Sensors*, vol. 16, no. 9, 2016, Art. no. 1505.
[5] T. Schuster, C. G. Schaffer, M. Mertig, and M. Bonsch, "Fiber grating-assisted investigation on surface plasmon resonance of fiber cladding modes," in *Proc. IEEE Sens.*, 2012, vol. 5855, pp. 1–4.
[6] E. Fontana, H. D. Dulman, D. E. Doggett, and R. H. Pantell, "Surface plasmon resonance on a single mode fiber," *IEEE Instrum. Meas. Technol. C*, vol. 1, no. no. 1, pp. 611–616, Feb. 2002.
[7] C. Caucheteur, F. Lhommé, K. Chah, M. Blondel, and P. Mégret, "Fiber Bragg grating sensor demodulation technique by synthesis of grating parameters from its reflection spectrum," *Opt. Commun.*, vol. 240, pp. 329–336, 2004.
[8] B. B. Shuai, X. Li, Y. Z. Zhang, and D. M. Liu, "A multi-core holey fiber based plasmonic sensor with large detection range and high linearity," *Opt. Express*, vol. 20, pp. 5974–5986, 2012.
[9] S. Ma, W. Li, H. Hu, and N. K. Dutta, "High speed ultra short pulse fiber ring laser using photonic crystal fiber nonlinear optical loop mirror," *Opt. Commun.*, vol. 285, no. 12, pp. 2832–2835, 2012.
[10] A. Agrawal, N Kejalakshmy, B. M. A. Rahman, and K. T. V. Grattan, "Soft glass equiangular spiral photonic crystal fiber for supercontinuum generation," *IEEE Photon. Technol. Lett.*,vol. 21, no. 22, pp. 1722–1724, Nov. 2009.
[11] Y. Lu, C. J. Hao, B. Q. Wu, M. Musideke, and L. C. Duan, "Surface plasmon resonance sensor based on polymer photonic crystal fibers with metal nanolayers," *Sensors*, vol. 13, pp. 956–965, 2013.
[12] A. A. Rifat, R. Ahmed, G. A. Mahdiraji, and F. R. M. Adikan, "Highly sensitive D-shaped photonic crystal fiber based plasmonic biosensor in visible to near-IR," *IEEE Sens. J.*, vol. 17, no. 9, pp. 2776–2783, May 2017.
[13] G. Wang, S. Li, G. An, X. Wang, and Y. Zhao, "Highly sensitive D-shaped photonic crystal fiber biological sensors based on surface plasmon resonance," *Opt. Quantum Electron.*, vol. 48, no. 1, p. 46, 2016.
[14] N. N. Luan, R. Wang, W. H. Lv, and J. Q. Yao, "Surface plasmon resonance sensor based on D-shaped microstructured optical fiber with hollow core," *Opt. Express*, vol. 23, pp. 8576–8582, 2015.
[15] J. N. Dash and R. Jha, "On the performance of graphene-based D-shaped photonic crystal fibre biosensor using surface plasmon resonance," *Plasmonics*, vol. 10, pp. 1123–1131, 2015.
[16] G. An, S. Li, W. Qin, W. Zhang, and Z. Fan, "High-sensitivity refractive index sensor based on D-shaped photonic crystal fiber with rectangular lattice and nanoscale gold film," *Plasmonics*, vol. 9, pp. 1355–1360, 2014.
[17] S. Kita and T. Baba, "Refractive index sensing utilizing a cw photonic crystal nanolaser and its array configuration," *Opt. Express*, vol. 16, pp. 8174–8180, 2008.
[18] G. Govindan, S. G. Raj, and D. Sastikumar, "Measurement of refractive index of liquids using fiber optic displacement sensors," *J Amer. Sci.,* vol. 5, pp. 13–17, 2009.
[19] X. Chen, L. Xia, and C. Li, "Surface plasmon resonance sensor based on a novel D-shaped Photonic Crystal Fiber for low refractive index detection," *IEEE Photon. J.*, vol. 10, no. 1, 2018, Art. no. 6800709.
[20] D. Gao, C. Y. Guan, Y. W. Wen, X. Zhong, and L. B. Yuan, "Multi-hole fiber based surface plasmon resonance sensor operated at near-infrared wavelengths," *Opt. Commun.*, vol. 313, pp. 94–98, 2014.
[21] A. Hassani and M. Skorobogatiy, "Design criteria for microstructured optical fiber based surface plasmonresonance sensors," *J. Opt. Soc. Amer. B.* vol. 24, pp. 1423–1429, 2007.
[22] A. Csaki, F. Jahn, I. Latka, T. Henkel, and D. Malsch, "Nanoparticle layer deposition for plasmonic tuning of microstructured optical fibers," *Small*, vol. 6, pp. 2584–2589, 2010.
[23] A. Hassani and M. Skorobogatiy, "Photonic crystal fiber-based plasmonic sensors for the detection of bio-layer thickness," *J. Opt. Soc. Amer. B*, vol. 26, pp. 1550–1557, 2009.
[24] X. Yu, Y. Zhang, S. S. Pan, P. Shum, M. Yan, Y. Leviatan, and C. M. Li, "A selectively coated photonic crystalfiber based surface plasmon resonance sensors," *J. Opt.* vol. 12, pp. 015005–015011, 2010.
[25] S. Zhang *et al.*, "Theoretical study of dual-core photonic crystal fibers with metal wire," *IEEE Photon. J.* vol. 4, no. 4, pp. 1178–1187, Aug. 2012.
[26] P. D. Mcintyre and A. W. Snyder, "Power transfer between optical fibers," *J. Opt. Soc. Amer.*, vol. 63, pp. 1518–1527, 1973.
[27] G. Ren, S. Lou, F. Yan, and S. Jian, "Mode interference in dual-core photonic crystal fibers," *Proc. SPIE.*, vol. 5623, pp. 129–132, 2005.
[28] Z Luo, T. Suyama, X. Xu, and Y. Okuno, "A grating-based plasmon biosensor via phase detection with wide measurement range," *Piers Proc.* vol. 5, pp. 974–978, 2013.
[29] C. Liu *et al.*, "Design and theoretical analysis of a photonic crystal fiber based on surface plasmon resonance sensing," *J. Nanophoton.*, vol. 9, 2015, Art. no. 093050.
[30] P. Bing, Z. Li, and J. Yao, "Effects of heterogeneity on the surface plasmon resonance biosensor based on three-hole photonic crystal fiber," *Opt. Eng.*, vol. 52, pp. 532–543, 2013.
[31] A. Csaki, F. Jahn, I. Latka, T. Henkel, and D. Malsch, "Nanoparticle layer deposition for plasmonic tuning of microstructured optical fibers," *Small*, vol. 6, pp. 2584–2589, 2010.